Theoretical analysis of FMR-driven spin pumping current and its properties via the self-consistent harmonic approximation

A. R. Moura ⓘ[*]

Departamento de Física, Universidade Federal de Viçosa, 36570-900, Viçosa, Minas Gerais, Brazil

We applied the self-consistent harmonic approximation (SCHA), combined with coherent states formalism, to study the ferromagnetic resonance (FMR) in a ferromagentic/normal metal junction. Due to the interface interaction, the FMR-generated spin current is injected from the magnetic insulator to the normal metal, the so-called spin pumping. Ordinarily, ferromagnetic models are described by bosonic representation or phenomenological theories; however, in a coherent magnetization state, the SCHA is the more natural choice to treat FMR problems. Over the years, the SCHA has successfully applied to investigate ferro- and antiferromagnetism in a wide range of scenarios. The main point of the SCHA formalism involves the adoption of a quadratic model for which corrections are included through temperature-dependent renormalization parameters. Therefore the SCHA is an efficient method for determining the properties of magnetically ordered phases. Using the SCHA, we obtained the temperature dependence of FMR-driven spin pumping. In addition, we found the spin-mix conductance, the additional damping from the angular momentum injection into the normal metal side, and the magnetic susceptibility. The SCHA outcomes are in remarkable agreement with the results of the literature.

I. INTRODUCTION AND MOTIVATION

The manipulation of spin currents is crucial in spintronic research and has been a topic of great interest due to its potential application in new spin-based technologies [1,2]. By definition, spin current involves an effective transport of angular momentum and, opposite to the conventional (electrical) charge current, the spin current can also be achieved in insulating materials. A spin current is obtained in conductors when up- and down-oriented electron spin fluxes show different densities, as occurs in the spin Hall effect [3] or using spin valves for filtering one of the spin-oriented conduction electrons, for example. On the other hand, in magnetic insulators, the spin transport is provided by magnons (the quanta of spin wave) [2,4] or even spinons (neutral half-integer spin excitation) [5–7]. Since the current in insulators does not involve charge transport, it is defined as a pure spin current.

When considering the interface between a normal metal (NM) and a magnetic material (here considered a ferromagnetic insulator, FMI) in a junction, two processes deserve special attention. The first one is related to the spin current injection from the conductor to the magnetic side due to the spin accumulation on the normal metal close to the interface, termed spin-transfer torque (SST) [8,9]. Then, in this case, the angular momentum injection can induce the magnetization to precess around the ordered axis or even revert its orientation. On the other hand, the opposite process, named spin pumping (SP), involves the injection of pure spin current from the magnetic side to the conductor [10]. The SP process can be provided by ferromagnetic resonance (FMR)

or electron paramagnetic resonance (EPR), depending on the magnetic sample [11]. In both processes, a resonant magnetic field induces the magnetization to precess and emit angular momentum that is propagated via spin waves. In addition, due to the magnon absorption, conduction electrons close to the interface are scattered through a spin-flip process. The EPR/FMR-driven spin pumping is frequently detected on the conductor side by using a metal with strong spin-orbit coupling. Therefore, due to the inverse spin Hall effect (ISHE) [12,13], the spin current injected is converted into a charge current that provides a dc voltage on the metal. A detailed explanation of SST and SP processes can be found in Refs. [4,14].

Usually, in addition to the phenomenological description through the Landau-Lifschitz-Gilbert (LLG) equation [10,15–19], STT and SP processes have been investigated by adopting Green functions and bosonic representations to describe the magnetic material [20–23]. The Holstein-Primakoff representation [24,25] allows representing the spin operators as first-order creation/annihilation operators only in the magnon low-occupation limit. On the order hand, if magnon interactions are relevant, higher-order terms should be considered, which introduce complications in the development. In the SU(N) Schwinger [25–27] representation, each spin component is represented by pair combinations involving N flavors of bosonic operators, which results in a four-order Hamiltonian. The quartic-order Hamiltonian terms are then decoupled by introducing auxiliary fields (a mean-field approximation) whose values are determined by solving coupled self-consistent equations. The Schwinger formalism provides good results in both ordered and disordered phases; however, in frustrated models, including Gaussian fluctuations becomes necessary [28–31]. In addition, extra care is required,

---

[*]antoniormoura@ufv.br

mainly for three-dimensional models close to the transition temperature [32]. The self-consistent Gaussian approximation (SCGA) [33] presents a purpose similar to the self-consistent harmonic approximation (SCHA). In the SCGA, the thermodynamics of a classical spin model is evaluated through self-consistent equations depending on the magnetization and their quadratic fluctuations. In this case, the Gaussian corrections are introduced by considering spin cumulants [34,35] in the statistical averages. The SCGA formalism provides good results; however, the number of self-consistent parameters is larger than the SCHA, and the quantization is more challenging to implement. On the other hand, the SCHA provides a simple quadratic method in which corrections are implemented by renormalization parameters depending on temperature. The renormalization parameters are self-consistently determined in order to give the best harmonic approximation in terms of S^z spin component and its conjugated angle φ. More details about the SCHA formalism are given in Sec. III.

In FMR experiments, the magnetization precession exhibits a coherent phase of the spin field just like the electromagnetic field does in a LASER. In this case, the entire spin field shows synchronous dynamics and can be represented by using a single spin that is well pictured by a classical vector. A quantum state like that is formally described by a coherent state, which was initially used to derive a fully quantum model of the radiation fields [36,37] as well as the coherent behavior of magnons [38–40]. It is well-known that coherent states represent the more classical-quantum state, i.e., states with minimum uncertainty [41]. Consider, for example, a particle in a harmonic potential and represented by a coherent state. In this case, $\Delta x \Delta p = \hbar/2$, while the wave function describes a dispersionless wave packet that moves harmonically around the minimum of the potential. Similar semi-classical behavior is reached for the spin field in the FMR. Then, we represent the spin by the phase angle φ around the z-axis and the conjugate momentum associated, namely S^z. In some cases, S^z is aligned with the magnetization direction, but this is unnecessary. Here, we define S^z and S^y as transverse components throughout the text, while the magnetization is along the x-axis as shown in Fig. 1. Note that $\varphi \ll 1$ and thus, the transverse spin components S^y and S^z are much smaller that the longitudinal component S^x. In addition, provided that $S^z \propto \dot{\varphi}$, both fields φ and S^z show an oscillating behavior during the magnetization precession as it is explained in next section. From the classical point of view, the fields φ_i and S^z_j, on sites i and j, respectively, satisfy the Poisson bracket $\{\varphi_i, S^z_j\} = \delta_{ij}$, and the quantization is achieved by promoting the fields to operators that obey the commutation relation $[\varphi_i, S^z_j] = \delta_{ij}$. Similar to the particle case, the operators obey the local equality $\Delta\varphi\Delta S^z = 1/2$, which justifies the semiclassical magnetization behavior of the spin. Therefore it is natural to adopt φ and S^z as the fundamental operators for describing magnetic models in FMR experiments instead of the usual bosonic representations.

Over the years, the self-consistent harmonic approximation has been successfully applied to evaluate the critical temperature [42–47], the topological BKT transition [42,45,48–58], and the large-D quantum phase transition [59–63] in a wide variety of magnetic models. In the SCHA
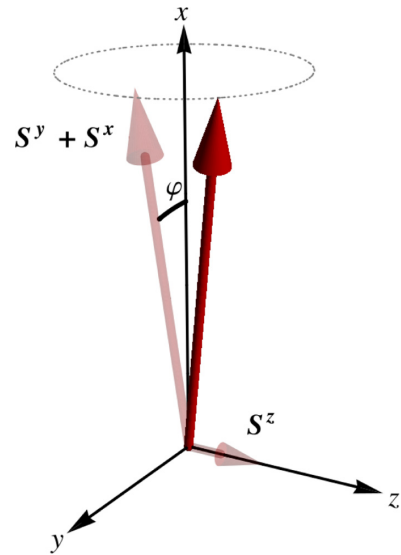

FIG. 1. The magnetization is aligned along the x axis (the direction of a static magnetic field B^x) and $S^y, S^z \ll S^x$. Here, φ is defined as the angle between the spin projection on the xy plane and the x axis.

formalism, the Hamiltonian is expanded to second order in φ and S^z operators, while higher-order contributions are included through temperature-dependent renormalization parameters. In addition, Moura and Lopes have demonstrated that SCHA is entirely compatible with the coherent state approach [64]. Therefore the SCHA formalism is the most plausible choice for studying the magnetization precession phenomena. In this work, we used the SCHA formalism to provide a new framework for the FMR-driven spin pumping across an NM/FMI junction interface. As primary outcomes, we obtain the FMR-driven spin current across the interface, the spin-mixing conductance, the additional Gilbert damping due to the angular momentum injection, and the magnetic susceptibility. All our results are in excellent agreement with well-known results in the literature.

II. MODEL DESCRIPTION

In the present work, we consider a NM/FMI junction. The ferromagnetic material is a thin film with the magnetization axis (defined as the x axis) normal to the film plane, as shown in Fig. 2. After minor modifications, the case whose magnetization is parallel to the plane could also be investigated through the SCHA formalism. The electronic side is considered a nonmagnetic spin sink, as platinum. For a poor spin sink, the conduction-electron spin-diffusion length is large, and a spin accumulation takes place close to the interface, which results in a spin black-flow into the FMI [17,65]. However, we are mainly concerned with the spin pumping process, which we consider a perfect spin sink, and conduction electrons rapidly decay after spin-flip scattering at the interface. Therefore there is no relevant spin accumulation, and the spin back-flow can be disregarded. In addition, bulk electronic interactions are also supposed to be unessential, and a free electron model represents the normal metal.
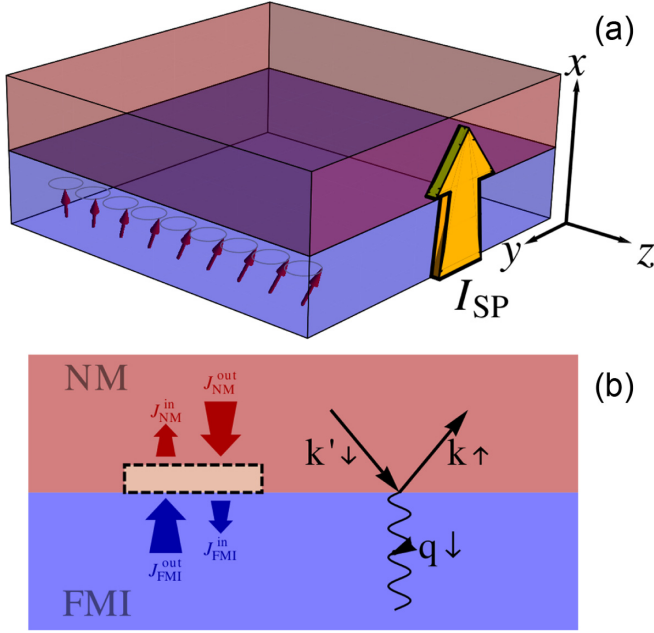
FIG. 2. (a) The NM/FMI junction and the adopted orientation of the axis. (b) The spin current across a pillbox at the FMI/NM interface, and the diagram representing the interface representation.

Conduction electrons interact with localized electrons at the interface through an sd-exchange potential [20,66]. Thus the Hamiltonian is written as the sum $H = H^m + H^e + H^{sd}$, where H^m, H^e, and H^{sd} are the magnetic, electronic, and interface contributions, respectively. The usual ferromagnetic Heisenberg model gives the magnetic Hamiltonian

$$H^m = -\frac{J}{2} \sum_{\langle ij \rangle} \mathbf{S}_i \cdot \mathbf{S}_j - g\mu_B \sum_i \mathbf{S}_i \cdot \mathbf{B}_i(t), \qquad (1)$$

where $J > 0$ is the exchange coupling, and the first sum is done over nearest neighbors. $\mathbf{B}_i(t) = \mu_0(H_i^x - N_x M_x)\hat{i} + \mu_0 H_i^y(t)\hat{j} + \mu_0 H_i^z(t)\hat{k}$ is the effective magnetic field, which is composed of the external field $\mathbf{H}$ and the demagnetizing field oriented along the x axis. M_x is the normal magnetization and, due to the adopted geometry, $N_x = 1$, while $N_y = N_z = 0$. In the above equation, H_i^x is a constant field responsible for aligning the spin field while the transverse components, $H_i^{y,z}(t)$, are oscillating fields that induce the magnetization precession. Here, we have included only the terms necessary to reach the coherent behavior; however, other contributions, such as different anisotropies, can be implemented to improve the model. As will be justified in the next section, the axis was chosen to provide a simpler development in the SCHA formalism. In the many-body representation, the electronic Hamiltonian is expressed as

$$H^e = \sum_{k\sigma} \epsilon_k c_{k\sigma}^\dagger c_{k\sigma}, \qquad (2)$$

where $\epsilon_k = \hbar^2 k^2/2m$, $c_{k\sigma}$ $(c_{k\sigma}^\dagger)$ is the annihilation (creation) electron operator, and $\sigma = \uparrow, \downarrow$ is the spin index. Here, as usual, we adopt electron spins aligned along the magnetization direction (x axis). Therefore the electron states are defined as the eigenstates of σ_x. Finally, the interface interaction is

given by

$$H^{sd} = 2J_{sd} \sum_i \mathbf{s}_i \cdot \mathbf{S}_i, \qquad (3)$$

where $J_{sd} < 0$ is the coupling between conduction and localized electrons, s_i is the conduction electron spin operator, S_i is the spin of localized electrons on the FMI, and the sum is done over the interface sites. As we will see in the following sections, the injected spin current is highly dependent on the sample properties, including the interface coupling. Since sd-exchange is sensitive to the electron distance interaction, it is not easy to stipulate an exact value over the entire surface. An estimated value for the sd coupling is of the order of -0.1 eV [67]. In addition, $\mathbf{s}_i = \psi_i^\dagger \boldsymbol{\sigma} \psi_i$, where $\psi_i^\dagger = (c_{i\uparrow}^\dagger \; c_{i\downarrow}^\dagger)$ is the electron spinor and σ is a vector whose components are given by the Pauli matrices. Using the basis of σ_x eigenstates, in the momentum space, H^{sd} is written as

$$H^{sd} = \sum_{kk'q} \Lambda_{kk'q} S_q^+ c_{k'\downarrow}^\dagger c_{k\uparrow} + \text{H.c.} \qquad (4)$$

with $S_q^+ = S_q^y + iS_q^z$ and

$$\Lambda_{kk'q} = \frac{J_{sd}}{N_e \sqrt{N_m}} \sum_i e^{i(\mathbf{k}-\mathbf{k}'-\mathbf{q})\cdot \mathbf{r}_i}, \qquad (5)$$

where N_e and N_m are the number of conduction electrons and magnetic sites, respectively. In the above equation, we consider only the terms that imply spin-flip scattering (related to the spin transverse components). The longitudinal term $s_i^x S_i^x$ involves number particle conservation scatterings and does not contribute to the spin current across the interface. Indeed, the injection (or absorption) of angular momentum is related to a change of the magnetization component along the angular momentum direction (M^x in our case). It is possible only for interaction terms that includes the S^+ and S^- ladder operators. In addition, the spin-flip scattering is related to the spin-mixing conductance, which arises in the LLG formalism and represents the transparency of the spin current across the interface [10,17].

III. SCHA FORMALISM

As commented previously, in the coherent magnetization phase, the more natural spin representation is done by using φ and S^z as fundamental operators, which is achieved through the Villain representation $S_i^+ = e^{i\varphi_i}\sqrt{\tilde{S}^2 - S_i^z(S_i^z + 1)}$, where $\tilde{S} = \sqrt{S(S+1)}$ [68]. Therefore one can always expand the spin components up to second order in φ and S^z to provide the spin-wave spectrum energy without any correction. However, better results are obtained with the inclusion of renormalization parameters that consider the contributions of higher-order terms. In the SCHA, we include a renormalization factor ρ for each term that presents a phase expansion. Therefore, in the series expansion, we replace φ by $\sqrt{\rho}\varphi$. The renormalization parameters are then found by solving a set of self-consistent equations. Here, we treat the time-dependent term of the magnetic Hamiltonian as a potential, solved in Sec. IV, while the

quadratic model represents the constant contribution

$$H_0^m = \frac{J}{2} \sum_{\langle ij \rangle} \left(\frac{\rho_E \tilde{S}^2}{2} \Delta\varphi^2 + S_i^z S_i^z - S_i^z S_j^z \right)$$
$$+ \frac{g\mu_B B_x}{2} \sum_i \left(\rho_B \tilde{S} \varphi_i \varphi_i + \frac{1}{\tilde{S}} S_i^z S_i^z \right), \quad (6)$$

where we adopt a uniform field H^x, $\Delta\varphi = \varphi_j - \varphi_i$, and include one factor renormalization for each φ expansion. Generally, $\rho_E \lesssim \rho_B$, and both parameters abruptly vanish at the same critical temperature. In momentum space, the Hamiltonian assumes the simple quadratic form

$$H_0^m = \frac{1}{2} \sum_q \left(h_q^\varphi \rho_{\text{eff}} \tilde{S}^2 \varphi_{-q} \varphi_q + h_q^z S_{-q}^z S_q^z \right), \quad (7)$$

where $\rho_{\text{eff}} = \sqrt{\rho_E \rho_B}$ is an effective renormalization parameter, the coefficients are given by

$$h_q^\varphi = zJ(1 - \gamma_q) \sqrt{\frac{\rho_E}{\rho_B}} + \frac{g\mu_B B_x}{\tilde{S}} \sqrt{\frac{\rho_B}{\rho_E}}, \quad (8a)$$

$$h_q^z = zJ(1 - \gamma_q) + \frac{g\mu_B B_x}{\tilde{S}}, \quad (8b)$$

and $\gamma_q = z^{-1} \sum_\eta e^{i\mathbf{q}\cdot\eta}$ is the factor structure of z nearest-neighbor spins located at η positions. Note that, using the ansatz $S_q^y \approx \sqrt{\rho_{\text{eff}}} \tilde{S} \varphi_q$, we can write the Hamiltonian in terms of fluctuations of the transverse spin components as $H_0^m = (1/2) \sum_q (h_q^\varphi S_{-q}^y S_q^y + h_q^z S_{-q}^z S_q^z)$. From the semiclassical analysis, the spin dynamics is obtained from the Hamilton equations $\dot{\varphi}_{-q} = -\partial H / \partial S_q^z$ and $\dot{S}_{-q}^z = \partial H / \partial \varphi_q$, which provide the transverse spin component dynamics

$$\dot{S}_q^y = -\sqrt{\rho_{\text{eff}}} \tilde{S} h_q^z S_q^z, \quad (9a)$$

$$\dot{S}_q^z = \sqrt{\rho_{\text{eff}}} \tilde{S} h_q^\varphi S_q^y. \quad (9b)$$

Assuming the elliptical oscillating transverse behavior, i.e., $S_q^y(t) = A_q^y \cos(\omega_q t)$ and $S_q^z(t) = A_q^z \sin(\omega_q t)$, where $A_q^{y,z}$ are the transverse amplitudes, it is easy to obtain the spin-wave frequencies, given by $\omega_q = \tilde{S}\sqrt{\rho_{\text{eff}} h_q^\varphi h_q^z}$.

To diagonalize the quantum Hamiltonian, we define bosonic operators via

$$\varphi_q = \frac{1}{\sqrt{2}} \left(\frac{h_q^z}{\rho_{\text{eff}} \tilde{S}^2 h_q^\varphi} \right)^{1/4} (a_q^\dagger + a_{-q}), \quad (10a)$$

$$S_q^z = \frac{i}{\sqrt{2}} \left(\frac{\rho_{\text{eff}} \tilde{S}^2 h_q^\varphi}{h_q^z} \right)^{1/4} (a_q^\dagger - a_{-q}), \quad (10b)$$

which results in $H_q^m = \sum_q E_q a_q^\dagger a_q$, where

$$E_q = \hbar\omega_q = \tilde{S}\sqrt{\rho_{\text{eff}} h_q^\varphi h_q^z} \quad (11)$$

are the magnon eigenenergies, in agreement with the semiclassical result. In addition, it is a straightforward procedure to get the Holstein-Primakoff-like ladder operators

$$S_q^+ \approx \sqrt{\rho_{\text{eff}}} \tilde{S} \varphi_q + i S_q^z = \sqrt{2\tilde{S}} \rho_{\text{eff}}^{1/4} b_q, \quad (12)$$

and $S_q^- \approx \sqrt{2\tilde{S}} \rho_{\text{eff}}^{1/4} b_q^\dagger$, where we define

$$b_q = \cosh\theta_q a_q + \sinh\theta_q a_{-q}^\dagger \quad (13)$$

with the angle θ_q is determined from

$$\tanh\theta_q = \frac{\sqrt{h_q^z} - \sqrt{h_q^\varphi}}{\sqrt{h_q^z} + \sqrt{h_q^\varphi}}. \quad (14)$$

Note that states generated by the b operator are linear combinations of a states moving in opposite directions. Since a_q operators diagonalize the transverse spin component Hamiltonian, the a states represent modes with spin in the yz plane. In contrast, b states are magnons with spin along the x axis. When we disregarded the renormalization procedure (equivalent to adopt $\rho_E = \rho_B = 1$), we obtain $a_q = b_q$, provided that $\theta_q = 0$. Since $h_q^\varphi = h_q^z$, the Hamiltonian can be written only in terms of $S_{-q}^x S_q^x$, and it is natural to consider spin fluctuation along the longitudinal direction. The renormalization parameters are given by

$$\rho_E = \left(1 - \frac{\langle S_i^z S_i^z \rangle_0}{\tilde{S}^2} \right) e^{-\frac{1}{2}\langle \Delta\varphi^2 \rangle_0} \quad (15)$$

and

$$\rho_B = \left(1 - \frac{\langle S_i^z S_i^z \rangle_0}{2\tilde{S}^2} \right) e^{-\frac{1}{2}\langle \varphi_i \varphi_i \rangle_0}, \quad (16)$$

where the indexes E and B states for the exchange and the static magnetic field (B^x) contribution, respectively. A quick demonstration of the above equations is given in Appendix A. In addition, to determine ρ_E and ρ_B, we must also resolve the equation of the magnetization $M^x = (g\mu_B/a^3)\langle S^x \rangle$, where a^3 is the unit cell volume and

$$\langle S^x \rangle = \frac{1}{2}\langle (S^+ + S^-) \rangle_0 \approx \tilde{S}\rho_B. \quad (17)$$

At finite temperatures, the expected values are determined by the statistical average using Eq. (10). At a critical temperature T_c, both parameters abruptly drop to zero, and so the SCHA is suitable only for $T < T_c$.

IV. MAGNETIC COHERENT STATE

The static (H^x) and dynamic (H^y and H^z) components of field **H** are fundamental pieces to provide the FMR-driven spin pumping. In a typical FMR experiment, an alternating field at microwave frequencies forces the spin field to oscillate around the direction defined by the static field perpendicular to the dynamic one. While the frequency Ω of the oscillating field is kept constant, the static field is adjusted to provide the resonance condition of the excited magnons, i.e., $\Omega = \omega_{q=0}$. When the resonance condition is achieved, the entire spin field oscillates in the synchronous behavior, which defines the coherent magnetization state. In this section, we show that the SCHA provides an efficient formalism to describe the coherent phase of FMR experiments.

To adequately describe the role of the oscillating field, we consider the Zeeman energy associated with it as a time-

dependent potential expressed, in the momentum space, as

$$V(t) = -\frac{g\mu_B\sqrt{2\tilde{S}}}{2}\sum_q[S_q^+B_q^-(t) + S_q^-B_q^+(t)], \qquad (18)$$

where $B_q^+(t) = B_q^y(t) + iB_q^z(t) \equiv B_qe^{-i\Omega t}$. The time evolution is then written as $\hat{A}(t) = S^\dagger(t)\hat{A}_0(t)S(t)$, where

$$\hat{A}_0(t) = e^{\frac{i}{\hbar}K_0t}\hat{A}e^{-\frac{i}{\hbar}K_0t} \qquad (19)$$

with $K_0 = K_0^e + H_0^m$, and we define the time evolution operator

$$S(t) = T_t\exp\left[-\frac{i}{\hbar}\int_0^t\hat{V}_0(t')\right]dt'. \qquad (20)$$

In this case, opposite to the LRT procedure, it is unnecessary to expand the exponential in lower orders of $\hat{V}_0$. Using the Eq. (12), the exponential argument is expressed as $\sum_q(\bar{\alpha}_qa_q - \alpha_qa_q^\dagger)$, where the coefficient α_q is given by

$$\alpha_q = i\gamma\sqrt{2\tilde{S}}\rho_{\text{eff}}^{1/4}B_q\int_0^t(\cosh\theta_qe^{-i\Omega t'} + \sinh\theta_qe^{i\Omega t'})$$
$$\times e^{i(\omega_q+i\varepsilon)t'}dt', \qquad (21)$$

with $\varepsilon \ll \omega_q$ being an infinitesimal factor included to ensure the convergence for long times, and $\gamma = g\mu_B/\hbar$. The convergence factor plays the same role as a damping term, which was not considered *a priori* but can be added through a phenomenological analysis.

Usually, the NM/FMI samples are tiny, and the oscillating fields can be considered uniform over the magnetic material, which results in $B_q = \sqrt{N_m}B_\perp\delta_{q,0}$. In addition, since Ω is of the order of 10 GHz, we can adopt that $\Omega^{-1} \ll \varepsilon^{-1} \ll t$, which simplifies the integral result to the time-independent value $\alpha_q = \alpha_0\delta_{q,0}$, with

$$\alpha_0 = \gamma B_\perp\sqrt{2\tilde{S}N_m}\rho_{\text{eff}}^{1/4}\left(\frac{\cosh\theta_0}{\Omega - \omega_0 - i\varepsilon} - \frac{\sinh\theta_0}{\Omega + \omega_0 + i\varepsilon}\right). \qquad (22)$$

Therefore, provided the high frequency of the oscillating field, the system rapidly assumes a stationary regime with uniform magnetization precession. The time evolution operator, given by Eq. (20), assumes a time-independent limit when $\varepsilon t \gg 1$, and so we write $S(t \gg \varepsilon^{-1}) = D(\alpha)$, where

$$D(\alpha) = \exp\left[\sum_q(\alpha_qa_q^\dagger - \bar{\alpha}_qa_q)\right], \qquad (23)$$

is the displacement operator that defines a coherent state by $|\alpha\rangle = D(\alpha)|0\rangle$, with $|0\rangle$ being the vacuum state. At finite temperature, the thermodynamics of coherent states is given by the thermal coherent states [69,70], which asserts that statistical averages are obtained from $\langle\hat{A}\rangle = \text{Tr}(\rho_{cs}\hat{A})$, where $\rho_{cs} = D(\alpha)\rho_0D^\dagger(\alpha)$ defines the coherent state density matrix, with $\rho_0 = e^{-\beta K_0}/\text{Tr}\rho_0$. Therefore, using the property $D^\dagger(\alpha)a_qD(\alpha) = a_q + \alpha_q$, we obtain $\langle a_q\rangle = \alpha_q$, and $\langle a_q^\dagger a_q\rangle = n(E_q) + |\alpha_q|^2$, where $n(E_q) = (e^{\beta E_q} - 1)^{-1}$ is the Bose-Einstein distribution, which counts the thermal excited states, and $|\alpha_q|^2 = N_q$ is the number of modes in the condensate state (usually the $q = 0$ state). It is important to observe
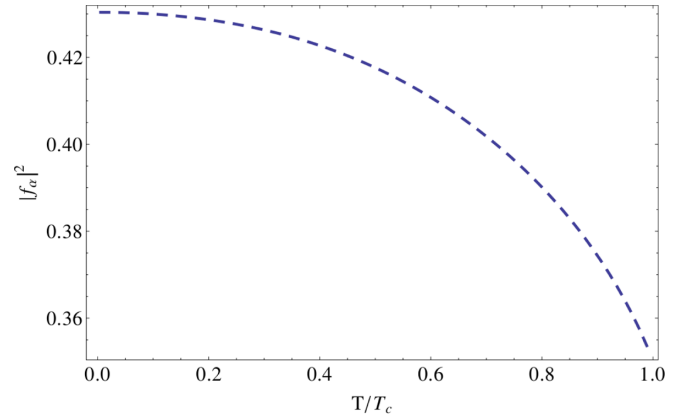

FIG. 3. The coherent occupation level $|f_\alpha|^2$ as function of the temperature. At $T = 0$, approximately 43% of the magnons are in the condensate state.

that in a coherent phase, a finite fraction of the particles (or excitation modes) occupy the same coherent state and $N_q \approx N$. In contrast, other states have a very low occupations, and we can disregard them.

Close to the resonance condition, we can use $\Omega \approx \omega_0$, and write $\alpha_0(T) = f_\alpha(T)\sqrt{N_m}$, where

$$f_\alpha(T) = \frac{\sqrt{2\tilde{S}}\gamma B_\perp\left(\rho_E^{1/4} + \rho_B^{1/4}\right)}{4(\Omega - \omega_0 - i\epsilon)}, \qquad (24)$$

measures the occupation of the coherent state. Replacing the infinitesimal parameter ϵ by $\eta_0\Omega$, where we adopt a typical value of the order of $\eta_0 \sim 10^{-3}$, we obtain $\gamma B_\perp/\eta\Omega \approx 1$, and so $|\alpha_0|^2 \approx 0.4N_m$. Note that a vanishing dissipation parameter implies in nonphysical behavior since the model acquires infinite energy due to the oscillating field. When the temperature increases, the number of magnons in the condensate phase decreases, and at $T = T_c$, the coherent state vanishes. For $T > T_c$, there is no mode in the condensate state, and magnetic excitations are composite only by thermal magnons (with distribution following the Bose-Einstein statistics). Figure 3 shows the dependence on the temperature of the occupation level. Curiously, even at zero temperature, only a fraction of the magnons participates in the coherent phase, similar to the physics of ^{4}He superfluid, for example.

The SCHA correctly describes the oscillating behavior of the transverse spin component when we consider the coherent state development. Indeed, using Eq. (10), we obtain the transverse magnetization dynamics

$$M_q^y(t) = A_q^y\cos(\Omega t - \phi_0), \qquad (25a)$$
$$M_q^z(t) = -A_q^z\sin(\Omega t - \phi_0), \qquad (25b)$$

where the transverse amplitudes are defined by $A_q^y = (g\mu_B/a^3)\sqrt{2\tilde{S}}\rho_E^{1/4}|\alpha_0|\delta_{q,0}$, and $A_q^z = (g\mu_B/a^3)\sqrt{2\tilde{S}}\rho_B^{1/4}|\alpha_0|\delta_{q,0}$, while ϕ_0 is the phase of α_0. Note that, due to the adopted representation, the magnetization shows a clockwise rotation, opposite to the usual counter clockwise direction. In addition, the averages present in the self-consistent
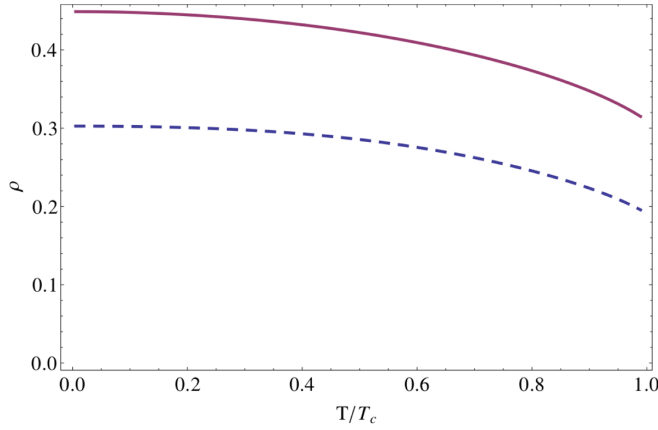
FIG. 4. The plot shows temperature dependence of the renormalization parameters ρ_E (dashed line) and ρ_B (solid line). $T_c = 1.83J/k_B$ is the critical temperature where the parameters abruptly vanish.

FIG. 5. The magnetization M^x (in units of H^x) of the ferromagnetic thin film below the critical temperature $T_c = 1.83J/k_B$.

equations are determined using

$$\langle S^z_{-q}S^z_q\rangle_{cs} = \frac{\tilde{S}}{2}\sqrt{\frac{\rho_{\text{eff}}h^\varphi_q}{h^z_q}}\coth\left(\frac{\beta\hbar\omega_q}{e}\right) + \langle S^z_q\rangle^2_{cs} \quad (26)$$

and

$$\langle\varphi_{-q}\varphi_q\rangle_{cs} = \frac{1}{2\tilde{S}}\sqrt{\frac{h^z_q}{\rho_{\text{eff}}h^\varphi_q}}\coth\left(\frac{\beta\hbar\omega_q}{2}\right) + \langle\varphi_q\rangle^2_{cs}, \quad (27)$$

where the hyperbolic cotangent term is related to the usual thermal fluctuations, while $\langle S^z_q\rangle^2_{cs}$ and $\langle\varphi_q\rangle^2_{cs}$ are finite only in the precession stat and measure the coherent phase. To solve the self-consistent equations, we also assume a time average and replace $\cos^2\Omega t$, and $\sin^2\Omega t$ by $1/2$. Considering $S = 1$, $\mu_0 H^x = 0.1T$, $\mu_0 H_\perp = 10^{-4}T$, and lattice spacing $a = 10^{-9}m$, we determine the renormalization parameters and its dependence on temperature is shown in Fig. 4. Both parameters abruptly drop to zero at the critical temperature $T_c = 1.83J/k_B$ and, for $T < T_c$, $\rho_E \lesssim \rho_B$. The critical temperature was determined considering the bcc lattice with a single ion per unit cell, and other configurations provide a different ratio $k_B T_c/J$. Here, we express the energies in units of J, and typical values of the exchange coupling are between 10^{-5} to 10^{-3} eV. Including anisotropic terms or other weak interactions also slightly changes the ratio $k_B T_c/J$. However, the results obtained from the simpler Hamiltonian (1) are in agreement with expected experimental measurements. We also determine the magnetization M^x dependence on temperature, and Fig. 5 shows the result obtained.

V. SPIN CURRENT THROUGH THE INTERFACE

The spin current across the interface can be evaluated on any side of the NM/FMI junction. Therefore, to determine the spin current, we consider a pillbox, on the NM side, in contact with the interface as shown in Fig. 2. The spin current across the pillbox boundary is composed of in and out components of spin current on the NM (J_{NM}) and FMI (J_{FMI}) sides. For a pillbox with a height much smaller than the conduction-electron spin-diffusion length, we can disregard
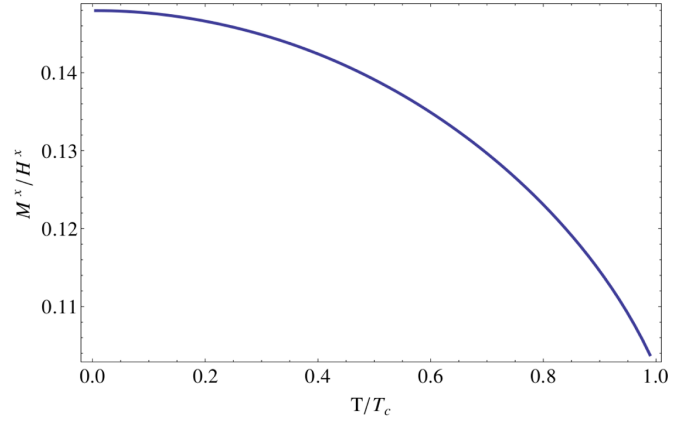
bulk spin-flip scattering, and the continuity equation provides $I_s = I_{\text{STT}} - I_{\text{SP}} = -(\hbar/2)\partial_t(N^e_\uparrow - N^e_\downarrow)$, where we define $I_{\text{STT}} = I^{(\text{in})}_{\text{FMI}} - I^{(\text{out})}_{\text{NM}}$ and $I_{\text{SP}} = I^{(\text{out})}_{\text{FMI}} - I^{(\text{in})}_{\text{NM}}$. Eventually, we will adopt conditions that vanish the spin current from the NM side, the STT contribution, and consider only the FMR-driven spin current. Thus, using the Heisenberg equation of motion, we obtain the spin current operator $I_s = i(A - A^\dagger)$, where

$$A^\dagger = \sum_{kk'q}\Lambda_{kk'q}S^+_q c^\dagger_{k'\downarrow}c_{k\uparrow}. \quad (28)$$

The expected value of the spin current is determined in the interaction picture by $\langle I_s(t)\rangle = \langle S^\dagger(t)\hat{I}_s(t)S(t)\rangle$, where the caret stands for time evolution according to the Hamiltonian $H - H^{\text{sd}}$, while, for small coupling at the interface, the time evolution operator $S(t)$ is approximated by

$$S(t) \approx 1 - \frac{i}{\hbar}\int^t_{-\infty}\hat{H}^{\text{sd}}(t')dt', \quad (29)$$

where we adopt an adiabatic evolution from $t \to -\infty$ (when $H^{\text{sd}} = 0$) to $t = 0$. Therefore the spin current is given by

$$I_s = \frac{2}{\hbar}\text{Im}\int^\infty_{-\infty}i\theta(t)\langle[\hat{A}(t),\hat{A}^\dagger(0)]\rangle dt. \quad (30)$$

Note that electronic states have time evolution according to H^e. At the same time, the statistical average, as usual, are evaluated using the grand canonical Hamiltonian $K^e = \sum_{k\sigma}\xi_{k\sigma}c^\dagger_{k\sigma}c_{k\sigma}$, where $\xi_{k\sigma} = \epsilon_k - \mu_\sigma$, and μ_σ is the chemical potential for electrons with spin σ. It is convenient to replace the time evolution to match with the Boltzmann weight, which provides

$$I_s = -2\text{Im}U_{\text{ret}}(\delta\mu), \quad (31)$$

where $\delta\mu = \mu_\uparrow - \mu_\downarrow$, and $U_{\text{ret}}(\delta\mu)$ is the time Fourier transform

$$U_{\text{ret}}(\delta\mu) = \int^\infty_{-\infty}U_{\text{ret}}(t)e^{\frac{i}{\hbar}\delta\mu t}dt \quad (32)$$

of the retarded function

$$U_{\text{ret}}(t) = -\frac{i}{\hbar}\langle[\hat{A}(t),\hat{A}^\dagger(0)]\rangle. \quad (33)$$

In the above equation, despite the same notation, the time evolution is defined by using K_e, while the electron energies are measured in relation to the chemical potential μ_σ. In this work, as we are interested in the FMR-drive spin current, from now on, we consider a perfect spin sink, which implies $\delta\mu = 0$, and consequently $I_{STT} = 0$. It is easy to obtain the retarded Green's function, whose magnetic part is now evaluated by using the coherent states obtained from the previous section. Using $\hat{A} = D^\dagger(\alpha)\hat{A}_0(t)D(\alpha)$, we have

$$U_{\rm ret}(t) = -\frac{i}{\hbar}\theta(t){\rm Tr}\big(D(\alpha)\rho_0 D^\dagger(\alpha)[\hat{A}_0^\dagger(t), \hat{A}_0(0)]\big)$$

$$= -\frac{i}{\hbar}\theta(t)\langle[\hat{A}_0(t), \hat{A}(0)]\rangle_{cs}, \qquad (34)$$

where the index cs refers to the coherent states of the magnetic Hamiltonian contribution. The averages on the normal metal are determined by using the usual Fermi-Dirac distribution.

VI. FMR-DRIVEN SPIN CURRENT

Once we have used the SCHA to obtain the coherent magnetization state, we can now determine the FMR-driven

spin current. Due to the dynamic field, the magnetization starts to precess, and coherent magnons fill the magnetic film transporting angular momentum over all directions. When a spin sink (the NM, in our case) is available, the spin current is allowed to leak across the NM/FMI interface. We apply Eq. (34) to Eq. (31) to evaluate the injected spin current, considering $\delta\mu = 0$ to avoid any contribution from spin backflow.

The retarded Green's function is generally determined by using the Matsubara formalism [66]. In this case, we use the imaginary time Green's function, defined by $\hbar\mathcal{U}(\tau) = -\langle T_\tau\hat{A}(\tau)\hat{A}^\dagger(0)\rangle$, to make the association in the Fourier space $\mathcal{U}(i\hbar\nu_n)|_{i\hbar\nu_n\to\delta\mu+i\varepsilon} = U_{\rm ret}(\delta\mu)$, where $i\hbar\nu_n = n\pi/\beta$ are the bosonic (fermionic) frequencies for n even (odd). However, the correspondence provided by the analytic continuation does not work when dealing with coherent states, and the retarded Green's function must be solved in real time formalism. The correspondence between the Matsubara and retarded Green formalisms fails due to the replacement of ρ_0 by ρ_{cs}. In this case, we can not use the same eigenvalues basis for ρ_{cs} and e^{iHt}, necessary condition to get the correspondence. Therefore the commutator present is $U_{\rm ret}(t)$ is determined in real time basis and given by

$$\langle[\hat{A}_0(t), \hat{A}^\dagger(0)]\rangle_{cs} = 2\tilde{S}\sqrt{\rho_{\rm eff}}\sum_{kk'q}|\Lambda_{kk'q}|^2(f_k - f_{k'})e^{\frac{i}{\hbar}(\xi_{k\uparrow} - \xi_{k'\downarrow})t}\big[\sinh\theta_q\cosh\theta_q\big(\bar{\alpha}_q^2 e^{i\omega_q t} + \alpha_q^2 e^{-i\omega t}\big)+$$

$$+ (n_q - n_{k-k'} + |\alpha_q|^2)(\cosh^2\theta_q e^{i\omega_q t} + \sinh^2\theta_q e^{-i\omega_q t})\big], \qquad (35)$$

where $n_q = (e^{\beta\hbar\omega_q} - 1)^{-1}$ and $n_{k-k'} = (e^{\beta(\xi_{k\uparrow} - \xi_{k'\downarrow})} - 1)^{-1}$ are Bose-Einstein distribution, while $f_k = (e^{\xi_{k\uparrow}} + 1)^{-1}$ $(f_{k'})$ is the Fermi-Dirac distribution for spin-up (spin-down) electrons. The second-order term

$$|\Lambda_{kk'q}|^2 = J_{sd}^2\sum_{ij}\frac{e^{i(\mathbf{k}-\mathbf{k'}-\mathbf{q})\cdot(\mathbf{r_j}-\mathbf{r_i})}}{N_e^2 N_m} \approx \frac{J_{sd}^2 N_{\rm int}}{N_e^2 N_m} \qquad (36)$$

is related to electrons and magnons that are created or annihilated at positions $\mathbf{r_i}$ and $\mathbf{r_j}$ on the interface. The approximation was adopted considering that particles are created and annihilated at close positions, and $N_{\rm int}$ is the number of sites at the interface.

Assuming $\delta\mu = 0$, the above equation is considerably simplified, and the imaginary part of the time Fourier transform is given by

$$\mathrm{Im}U_{\rm ret}(\delta\mu = 0) = -2\pi\tilde{S}\sqrt{\rho_{\rm eff}}\Bigg\{\bigg[|\alpha_0|^2\cosh^2\theta_0 + \frac{\alpha_0^2 + \bar{\alpha}_0^2}{2}\sinh\theta_0\cosh\theta_0\bigg]\sum_{kk'}(f_k - f_{k'})\delta(\epsilon_k - \epsilon_{k'} + \hbar\omega_0)+$$

$$+ \bigg[|\alpha_0|^2\sinh^2\theta_0 + \frac{\alpha_0^2 + \bar{\alpha}_0^2}{2}\sinh\theta_0\cosh\theta_0\bigg]\sum_{kk'}(f_k - f_{k'})\delta(\epsilon_k - \epsilon_{k'} - \hbar\omega_0)\Bigg\}. \qquad (37)$$

Considering the typical energy scale achieved in experimental arrangements, the electron momentum sum provides the simple result

$$\sum_{kk'}(f_k - f_{k'})\delta(\epsilon_k - \epsilon_{k'} \pm \hbar\omega_0) \approx \pm\frac{\rho_F^2\hbar\omega_0}{4}, \qquad (38)$$

where $\rho_F = (2m^3\epsilon_F)^{1/2}V/\pi^2\hbar^3$ is the density of states at the Fermi level (details can be see in Appendix B). Therefore the FMR-driven spin current density $(= I_{SP}/A)$ is given by

$$J_{SP}(T) = \left(\frac{J_{sd}\rho_F}{aN_e}\right)^2\pi\tilde{S}\hbar\omega_0|f_\alpha(T)|^2\sqrt{\rho_{\rm eff}(T)}, \qquad (39)$$

where we adopt a sample with interfacial area $A = L^2$. Figure 6 shows the FMR-driven spin pumping dependence on temperature. There is an apparent decrease with increasing temperature, which is expected provided by the reduction of magnetization coherence. It is important to emphasize that the temperature change is homogeneous over the junction, and we do not take into account the Seebeck effect, which comes from temperature gradients. In addition, above the critical temperature, SCHA predicts $\rho_E = \rho_B = 0$, which will result in a vanishing FMR-driven spin current; however, since the system shows a paramagnetic phase, a finite spin current could be provided from EPR. Both cases, FM with temperature gra-
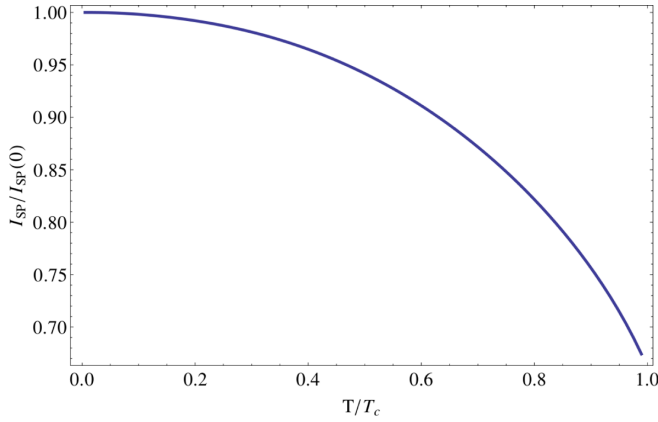
FIG. 6. The temperature dependence of the FMR-driven spin current for $0 \leqslant T \leqslant T_c$, where $T_c = 1.83J/k_B$ is the critical temperature in which ρ_E and ρ_B tend to zero.

dients and EPR-driven spin current, are fascinating problems. However, they demand a profound reformulation of the SCHA method, which is beyond the present work's scope.

To compare the SCHA outcomes with the well-known phenomenological results, we first briefly review the LLG equation endowed with the Slonczewski term [65], which is given by

$$\dot{\mathbf{m}} = -\gamma \mathbf{m} \times \mathbf{B}_{\text{eff}} + \eta_0 \mathbf{m} \times \dot{\mathbf{m}} + \boldsymbol{\tau}, \qquad (40)$$

where $\mathbf{m} = \mathbf{M}/M^s$ is the unity magnetization, $\mathbf{B}_{\text{eff}}$ is the effective magnetic field, η_0 is the bulk Gilbert damping, and $\boldsymbol{\tau} = (\gamma/M^s V_m)(\mathbf{m}_\perp \times \mathbf{I}_{SP} \times \mathbf{m}_\perp)$ is a torque due to the angular momentum leaking to the NM side. The LLG equation preserves the magnetization modulus; however, since the damping is small, we will consider an almost constant longitudinal magnetization component, while $\dot{\mathbf{m}} \approx \dot{\mathbf{m}}_\perp = \dot{\mathbf{m}}^y + \dot{\mathbf{m}}^z$. Another approach, which takes into account different damping from transverse and longitudinal magnetization components, is given by the Lifshitz-Landau-Bloch-Bloembergen (LLBB) equation [4,71–73]. Provided minor corrections, the SCHA method can also be applied to the LLBB equation as well. For a thick magnetic film, the injected spin current is related to the magnetization dynamics via

$$\mathbf{I}_{SP} = \frac{\hbar}{4\pi}(G_r^{\uparrow\downarrow} \mathbf{m} \times \dot{\mathbf{m}} - G_i^{\uparrow\downarrow} \dot{\mathbf{m}}), \qquad (41)$$

where $G^{\uparrow\downarrow} = G_r^{\uparrow\downarrow} + iG_i^{\uparrow\downarrow}$ is the dimensionless spin-mixing conductance, which can be determined from the scattering-matrix theory of transport [17]. In general, $G_r^{\uparrow\downarrow} \gg G_i^{\uparrow\downarrow}$ and, from now on, we will consider only the real part of $G^{\uparrow\downarrow}$. Therefore the spin current torque results in an additional contribution to the total Gilbert damping [19,21,74], which is written as $\eta = \eta_0 + \delta\eta$, where

$$\delta\eta = \frac{\gamma\hbar G^{\uparrow\downarrow}}{4\pi M^s V_m} \qquad (42)$$

is the extra damping from the FMR-driven spin current. It is more convenient to define the spin-mixing conductance per area $g^{\uparrow\downarrow} = G^{\uparrow\downarrow}/A$ and, for YIG films, typical spin-mixing conductance values are found over the interval $1.1 - 3.9 \times$

$10^{18} m^{-2}$, while $\eta_0 \sim 10^{-3}$, depending on geometric and intrinsic sample properties [75–77].

Using the transverse magnetization components obtained from SCHA, we get

$$(\mathbf{m} \times \dot{\mathbf{m}})^x = -\frac{(\gamma B_\perp)^2 \Omega (\rho_E^{1/4} + \rho_B^{1/4})^2 \sqrt{\rho_{\text{eff}}}}{4\tilde{S}[(\Omega - \omega_0)^2 + (\eta_0\Omega)^2]}, \qquad (43)$$

where the minus sign is related to the clockwise direction of the precession. Comparing the results of Eqs. (39) and (41), we obtain the spin-mixing conductance

$$g^{\uparrow\downarrow} = \frac{4\tilde{S}^3 J_{sd}^2 m_e^3 \epsilon_F}{\pi^2 \hbar^6 \rho_e^2 a^2}, \qquad (44)$$

where $\epsilon_F \sim 10$ eV is the Fermi energy, m_e is the electron mass, and $\rho_e \sim 10^{28}$ m^{-3} the NM electron density. For $J_{sd} \sim 0.1$ eV, and $a \sim 1$ nm, the above equation provides $g^{\uparrow\downarrow} \approx 2.6 \times 10^{18}$ m^{-2}, which is in remarkable agreement with experimental values. On the other hand, the additional Gilbert damping is given by

$$\delta\eta = \frac{m_e^3 a J_{sd}^2 \tilde{S}^2 \epsilon_F}{\pi^3 \hbar^6 \rho_e^2 d_m}, \qquad (45)$$

where d_m is the magnetic film thickness. For the same estimated parameters used above, and $d_m = 10^{-6}$ m, we found $\delta\eta \approx 1.5 \times 10^{-4}$, which is also within the expected.

Finally, we can also use the SCHA formalism to determine the magnetic susceptibility, which provides a valuable link between theory and experimental measurements [4]. Indeed, measurements from ISHE voltage in the NM side side directly correspond with the real and imaginary part of the magnetic susceptibility, and they are commonly used to get information about ferromagnetic damping. To obtain the susceptibility, we introduce the circularly polarized magnetization

$$M_q^+ = M_q^y + iM_q^z \approx \frac{g\mu_B}{a^3}\sqrt{2\tilde{S}}\rho_{\text{eff}}^{1/4}|\alpha_q|e^{-i(\Omega t - \phi_0)}, \qquad (46)$$

where we replace ρ_E and ρ_B by ρ_{eff} to simplify the result. Similarly, we define $B_q^+(t) = \sqrt{N_m}B_\perp\delta_{q,0}e^{-i\Omega t}$, which, after a simple calculation, provides

$$M_q^+(t) = \frac{\gamma M^s \sqrt{\rho_{\text{eff}}}}{\Omega - \omega_0 - i\eta_0\Omega}B_q^+(t). \qquad (47)$$

Since $B_q^+ = \mu_0(H_q^+ + M_q^+)$, we found $M_q^+ = \chi H_q^+$, with the magnetic susceptibility expressed by

$$\chi = \chi' + i\chi'' = \frac{\omega_M}{\Omega - \omega_H - i\eta_0\Omega}, \qquad (48)$$

where $\omega_H = \gamma\mu_0 H^x\sqrt{\rho_{\text{eff}}}$, and $\omega_M = \gamma\mu_0 M^s\sqrt{\rho_{\text{eff}}}$. Both real and imaginary parts of χ are shown in Fig. 7. Only to provide better visualization, we chose $\eta_0 = 10^{-2}$, and the vertical axis is normalized in terms of $\omega_M/\eta_0\Omega$. Apart from the renormalization factor, the magnetic susceptibility is identical to the well-known result found in the literature. The imaginary part of the susceptibility assumes half of the peak at the points $\omega_H = (1 \pm \eta_0)\Omega$, and the difference between them is used to define the linewidth ΔH (the same linewidth also be determined by the difference between the points that define the maximum and minimum of χ'). It is easy to demonstrate that
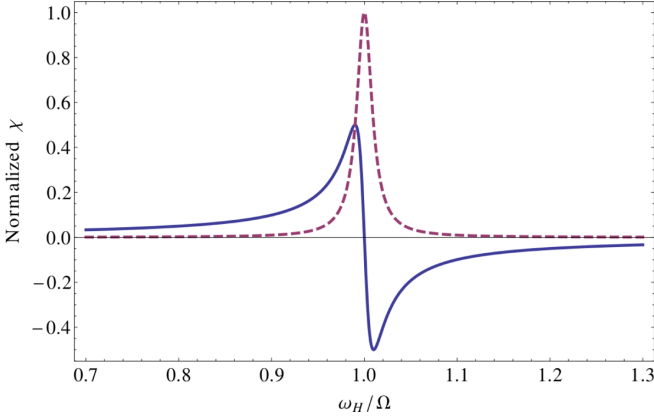
FIG. 7. The real (solid line) and imaginary (dashed line) parts of the magnetic susceptibility (normalized in terms of $\omega_M/\eta_0\Omega$) obtained from the SCHA formalism.

$\eta_0 = \sqrt{\rho_{\mathrm{eff}}}\gamma\,\Delta H/\Omega$ and so, the linewidth provides an alternative to determine the ferromagnetic damping. In addition, the imaginary part is proportional to the power absorption (per volume) of the oscillating field by the sample. Indeed, we can show that $P(\Omega) = \mu_0\Omega\chi''H_\perp^2/2$, and thus the absorption radiation is maximum close to the resonant condition $\omega_0 = \Omega$.

VII. SUMMARY AND CONCLUSIONS

In this work, we applied the SCHA formalism and coherent states to investigate the FMR-driven spin current in an NM/FMI junction. Over the years, similar problems have been analyzed through bosonic representations or phenomenological approaches. Provided the coherent nature of ferromagnetic resonance, it is appropriated to apply the coherent state formalism. In addition, in the SCHA formalism, the entire development is performed through the φ and S^z operators that satisfy $[\varphi_i, S_j^z] = \delta_{ij}$. Thus the SCHA is an advantageous method for studying problems involving FMR.

Here, we considered the application of a resonant driving field in an NM/FMI junction to provide the injection of spin current into the normal metal. First, the FMR-driven spin pumping was determined by using an sd coupling at the interface. Then, a precise and detailed development was performed to obtain, beyond the spin pumping current, the spin-mixing conductance, the extra magnetic damping from the spin pumping, and the susceptibility. The SCHA results showed considerable agreement with experimental data when considering typical experimental values of the involved parameters.

In summary, we have demonstrated the efficiency of the SCHA method, combined with coherent states, to treat magnetic problems in spintronics. Therefore a series of open problems could also be investigated by using the presented formalism that would result in a breakthrough for much spintronic research.

APPENDIX A: RENORMALIZATION PARAMETERES

To determine the renormalization parameter, we compare the value of $\langle \dot{S}_q^z\dot{S}_{-q}^z\rangle_0$ obtained from the quadratic Hamilto-

nian (7) with the result obtained from H^m without the series expansion. Starting with the former, and considering the semiclassical analysis, we obtain

$$\langle \hbar^2 \dot{S}_q^z\dot{S}_{-q}^z\rangle_0 = \left(h_q^\varphi \tilde{S}^2\right)^2 \langle \varphi_q\varphi_{-q}\rangle_0 = \frac{h_q^\varphi \tilde{S}^2}{\beta}, \qquad (A1)$$

with $h_q^\varphi = g\mu_B B^x\rho_B + zJ\tilde{S}^2(1-\gamma_q)\rho_E$. To find out the second term, given by the Fourier transform

$$\langle \dot{S}_q^z\dot{S}_{-q}^z\rangle = \frac{1}{N}\sum_{ij}\langle \dot{S}_i^z\dot{S}_j^z\rangle e^{i\mathbf{q}\cdot(\mathbf{r}_j-\mathbf{r}_i)}, \qquad (A2)$$

we use the following useful relation, obtained after an integration by parts,

$$\langle \hbar^2\dot{S}_i^z\dot{S}_j^z\rangle = \frac{1}{Z}\int \mathcal{D}\varphi\mathcal{D}S^z\frac{1}{\beta}\frac{\partial^2 H^m}{\partial\varphi_i\partial\varphi_j}e^{-\beta H^m}, \qquad (A3)$$

where Z is the partition function, and the integration measure $\mathcal{D}\varphi\mathcal{D}S^z$ stands for the field integration over each site on the lattice. In addition, we extend the integration limit to $-\infty < \varphi, S^z < \infty$ and thus we deal with Gaussian integrals. The derivative of the semiclassical Hamiltonian provides

$$\frac{\partial^2 H^m}{\partial\varphi_i\partial\varphi_j} = g\mu_B B^x\sqrt{\tilde{S}^2 - \left(S_i^z\right)^2}\cos\varphi_i\delta_{ij}$$

$$+ J\sum_l \sqrt{\tilde{S}^2 - \left(S_i^z\right)^2}\sqrt{\tilde{S}^2 - \left(S_l^z\right)^2}$$

$$\times \cos(\varphi_l - \varphi_j)(\delta_{ij} - \delta_{il}).$$

The Fourier transform is then written as

$$\langle \hbar^2\dot{S}_q^z\dot{S}_{-q}^z\rangle = \frac{g\mu_B B^x}{\beta}\langle\sqrt{\tilde{S}^2 - (S^z)^2}\cos\varphi\rangle$$

$$+ \frac{zJ(1-\gamma_q)}{\beta}\langle[\tilde{S}^2 - (S^z)^2]\cos\Delta\varphi\rangle, \quad (A4)$$

where we consider that the averages are site independent. Comparing with the previous result and using the decoupled quadratic Hamiltonian H_0^m to evaluate the average, we obtain the self-consistent equations used in the text.

APPENDIX B: ELECTRON MOMENTUM SUM

In order to evaluate the momentum sum of up- and down-spin, we use the conservation energy condition to write

$$\sum_k \delta(\epsilon_k - \epsilon_{k'} \pm \hbar\omega_0) \approx \frac{mV}{2\pi^2\hbar^2}k'\left(1 \pm \frac{\hbar\omega_0}{2\epsilon_{k'}}\right), \qquad (B1)$$

and thus, in the continuum limit, the left-hand side (l.h.s.) of Eq. (38) is given by

$$\frac{m^2V^2}{4\pi^3\beta\hbar^4}\left\{\frac{2m}{\beta\hbar^2}[F_1(\beta\mu \pm \beta\hbar\omega_0) - F_1(\beta\mu)]\right.$$

$$\left.\pm \frac{m\omega_0}{\hbar}[F_0(\beta\mu \pm \beta\hbar\omega_0) - F_0(\beta\mu)]\right\}, \qquad (B2)$$

where the integral was written as

$$\int\frac{d^3k'}{(2\pi)^3}\frac{f(\xi \pm \hbar\omega_0)}{k^{3-2l}} = \frac{\Gamma(l)}{4\pi}\left(\frac{2m}{\beta\hbar^2}\right)^l F_{l-1}(\beta\mu \mp \beta\hbar\omega_0) \tag{B3}$$

with

$$F_l(x) = \frac{1}{\Gamma(l+1)} \int_0^\infty dz z^l (e^{z-x} + 1)^{-1} \quad \text{(B4)}$$

being the complete Fermi-Dirac integral. Here, we have considered the perfect spin sink limit, i.e., $\mu_\uparrow = \mu_\downarrow = \mu$. For $l = 0$, we have the exact result $F_0(x) = \ln(1 + e^x)$, while the derivatives are given by $dF_l/dx = F_{l-1}(x)$. In usual FMR experiments, we deal with the energies $\mu \approx \epsilon_F \sim 10$ eV,

$k_B T \sim 10^{-2}$ eV, and $\hbar\omega_0 \sim 10^{-6}$ eV, which justify a Taylor expansion of the Fermi-Dirac integral F_1 around $\beta\mu$ (F_0 is assumed constant). Therefore Eq. (B2) provides

$$\sum_{kk'} (f_k - f_{k'}) \delta(\epsilon_k - \epsilon_{k'} \pm \hbar\omega_0) = \frac{m^3 V^2}{2\pi^4 \hbar^6} \frac{F_0(\beta\mu)}{\beta}, \quad \text{(B5)}$$

which directly results in Eq. (38).

[1] S. Wolf, D. Awschalom, R. Buhrman, J. Daughton, S. Von Molnar, M. Roukes, A. Y. Chtchelkanova, and D. Treger, Science **294**, 1488 (2001).

[2] I. Žutić, J. Fabian, and S. D. Sarma, Rev. Mod. Phys. **76**, 323 (2004).

[3] J. E. Hirsch, Phys. Rev. Lett. **83**, 1834 (1999).

[4] S. M. Rezende, *Fundamentals of Magnonics* (Springer, Switzerland, 2020), Vol. 969

[5] D. Hirobe, M. Sato, T. Kawamata, Y. Shiomi, K.-i. Uchida, R. Iguchi, Y. Koike, S. Maekawa, and E. Saitoh, Nat. Phys. **13**, 30 (2017).

[6] F. Lange, S. Ejima, T. Shirakawa, S. Yunoki, and H. Fehske, Phys. Rev. B **97**, 245124 (2018).

[7] D. Hirobe, T. Kawamata, K. Oyanagi, Y. Koike, and E. Saitoh, J. Appl. Phys. **123**, 123903 (2018).

[8] J. C. Slonczewski, J. Magn. Magn. Mater. **159**, L1 (1996).

[9] L. Berger, Phys. Rev. B **54**, 9353 (1996).

[10] Y. Tserkovnyak, A. Brataas, and G. E. W. Bauer, Phys. Rev. Lett. **88**, 117601 (2002).

[11] Y. Shiomi and E. Saitoh, Phys. Rev. Lett. **113**, 266602 (2014).

[12] A. Azevedo, L. Vilela Leao, R. Rodriguez-Suarez, A. Oliveira, and S. Rezende, J. Appl. Phys. **97**, 10C715 (2005).

[13] E. Saitoh, M. Ueda, H. Miyajima, and G. Tatara, Appl. Phys. Lett. **88**, 182509 (2006).

[14] A. Brataas, Y. Tserkovnyak, G. Bauer, and P. J. Kelly, Spin current **17**, 87 (2012).

[15] T. L. Gilbert, IEEE Trans. Magn. **40**, 3443 (2004).

[16] R. Urban, G. Woltersdorf, and B. Heinrich, Phys. Rev. Lett. **87**, 217204 (2001).

[17] Y. Tserkovnyak, A. Brataas, and G. E. W. Bauer, Phys. Rev. B **66**, 224403 (2002).

[18] A. Brataas, Y. Tserkovnyak, and G. E. W. Bauer, Phys. Rev. Lett. **101**, 037207 (2008).

[19] A. Kapelrud and A. Brataas, Phys. Rev. Lett. **111**, 097602 (2013).

[20] S. Takahashi, E. Saitoh, and S. Maekawa, *Journal of Physics: Conference Series* (IOP, 2010), Vol. 200, p. 062030.

[21] Y. Ohnuma, H. Adachi, E. Saitoh, and S. Maekawa, Phys. Rev. B **89**, 174417 (2014).

[22] S. Okamoto, Phys. Rev. B **93**, 064421 (2016).

[23] V. S. U. A. Vargas and A. R. Moura, Phys. Rev. B **102**, 024412 (2020).

[24] T. Holstein and H. Primakoff, Phys. Rev. **58**, 1098 (1940).

[25] A. Auerbach, *Interacting Electrons and Quantum Magnetism* (Springer Science & Business Media, 2012).

[26] D. P. Arovas and A. Auerbach, Phys. Rev. B **38**, 316 (1988).

[27] S. Sarker, C. Jayaprakash, H. R. Krishnamurthy, and M. Ma, Phys. Rev. B **40**, 5028 (1989).

[28] A. E. Trumper, L. O. Manuel, C. J. Gazza, and H. A. Ceccatto, Phys. Rev. Lett. **78**, 2216 (1997).

[29] M. G. Gonzalez, E. A. Ghioldi, C. J. Gazza, L. O. Manuel, and A. E. Trumper, Phys. Rev. B **96**, 174423 (2017).

[30] E. A. Ghioldi, M. G. Gonzalez, S.-S. Zhang, Y. Kamiya, L. O. Manuel, A. E. Trumper, and C. D. Batista, Phys. Rev. B **98**, 184403 (2018).

[31] S.-S. Zhang, E. A. Ghioldi, Y. Kamiya, L. O. Manuel, A. E. Trumper, and C. D. Batista, Phys. Rev. B **100**, 104431 (2019).

[32] M. D. Stiles and A. Zangwill, Phys. Rev. B **66**, 014407 (2002).

[33] D. A. Garanin, Phys. Rev. B **53**, 11593 (1996).

[34] G. Horwitz and H. B. Callen, Phys. Rev. **124**, 1757 (1961).

[35] R. Stinchcombe, G. Horwitz, F. Englert, and R. Brout, Phys. Rev. **130**, 155 (1963).

[36] R. J. Glauber, Phys. Rev. **131**, 2766 (1963).

[37] C. Gerry, P. Knight, and P. L. Knight, *Introductory Quantum Optics* (Cambridge University Press, 2005).

[38] S. M. Rezende and N. Zagury, Phys. Lett. A **29**, 47 (1969).

[39] N. Zagury and S. M. Rezende, Phys. Lett. A **29**, 616 (1969).

[40] N. Zagury and S. M. Rezende, Phys. Rev. B **4**, 201 (1971).

[41] W.-M. Zhang *et al.*, Rev. Mod. Phys. **62**, 867 (1990).

[42] A. S. T. Pires, A. R. Pereira, and M. E. Gouvêa, Phys. Rev. B **49**, 9663 (1994).

[43] A. Pires, Phys. Lett. A **202**, 309 (1995).

[44] A. R. Pereira, A. S. T. Pires, and M. E. Gouvea, Phys. Rev. B **51**, 16413 (1995).

[45] B. V. Costa, A. R. Pereira, and A. S. T. Pires, Phys. Rev. B **54**, 3019 (1996).

[46] A. S. T. Pires, Solid State Commun. **104**, 771 (1997).

[47] M. E. Gouvêa, G. M. Wysin, S. A. Leonel, A. S. T. Pires, T. Kamppeter, and F. G. Mertens, Phys. Rev. B **59**, 6229 (1999).

[48] S. Menezes, M. Gouvêa, and A. S. T. Pires, Phys. Lett. A **166**, 330 (1992).

[49] A. S. T. Pires and M. E. Gouvea, Phys. Rev. B **48**, 12698 (1993).

[50] A. S. T. Pires, Phys. Rev. B **50**, 9592 (1994).

[51] A. Pires, Solid State Commun. **100**, 791 (1996).

[52] A. S. T. Pires, Phys. Rev. B **53**, 235 (1996).

[53] A. S. T. Pires, Phys. Rev. B **54**, 6081 (1996).

[54] A. Pires, Solid State Commun. **112**, 705 (1999).

[55] A. S. T. Pires and M. Gouvêa, Eur. Phys. J. B **44**, 169 (2005).

[56] M. Gouvêa and A. Pires, physica status solidi (b) **242**, 2138 (2005).

[57] A. S. T. Pires, B. V. Costa, and R. A. Dias, Phys. Rev. B **78**, 212408 (2008).

[58] A. Pires, J. Magn. Magn. Mater. **452**, 315 (2018).

[59] A. Pires, Physica A **373**, 387 (2007).

[60] A. Pires, L. Lima, and M. Gouvea, J. Phys.: Condens. Matter **20**, 015208 (2008).

[61] A. Pires and M. Gouvea, Physica A **388**, 21 (2009).

[62] A. Pires and B. Costa, Physica A **388**, 3779 (2009).

[63] A. R. Moura, A. S. Pires, and A. R. Pereira, J. Magn. Magn. Mater. **357**, 45 (2014).

[64] A. R. Moura and R. J. C. Lopes, J. Magn. Magn. Mater. **472**, 1 (2019).

[65] Y. Tserkovnyak, A. Brataas, G. E. W. Bauer, and B. I. Halperin, Rev. Mod. Phys. **77**, 1375 (2005).

[66] G. D. Mahan, *Many-Particle Physics* (Springer Science & Business Media, 2013).

[67] J. Kondo, Prog. Theor. Phys. **32**, 37 (1964).

[68] J. Villain, Journal de Physique **35**, 27 (1974).

[69] A. Mann and M. Revzen, Phys. Lett. A **134**, 273 (1989).

[70] J. Oz-Vogt, A. Mann, and M. Revzen, J. Mod. Opt. **38**, 2339 (1991).

[71] N. Bloembergen, Phys. Rev. **78**, 572 (1950).

[72] N. Bloembergen and S. Wang, Phys. Rev. **93**, 72 (1954).

[73] O. Yalçın, *Ferromagnetic Resonance: Theory and Applications* (BoD-Books on Demand, Croatia, 2013).

[74] S. Rezende, R. Rodríguez-Suárez, M. Soares, L. Vilela-Leão, D. Ley Domínguez, and A. Azevedo, Appl. Phys. Lett. **102**, 012402 (2013).

[75] B. Heinrich, C. Burrowes, E. Montoya, B. Kardasz, E. Girt, Y.-Y. Song, Y. Sun, and M. Wu, Phys. Rev. Lett. **107**, 066604 (2011).

[76] R. Takahashi, R. Iguchi, K. Ando, H. Nakayama, T. Yoshino, and E. Saitoh, J. Appl. Phys. **111**, 07C307 (2012).

[77] C. Du, H. Wang, F. Yang, and P. C. Hammel, Phys. Rev. Appl. **1**, 044004 (2014).